# The B7-H3–Targeting Antibody–Drug Conjugate m276-SL-PBD Is Potently Effective Against Pediatric Cancer Preclinical Solid Tumor Models

Nathan M. Kendsersky[1,2], Jarrett Lindsay[1,2], E. Anders Kolb[3], Malcolm A. Smith[4], Beverly A. Teicher[4], Stephen W. Erickson[5], Eric J. Earley[5], Yael P. Mosse[1], Daniel Martinez[6], Jennifer Pogoriler[2,6], Kateryna Krytska[1], Khushbu Patel[1,7], David Groff[1], Matthew Tsang[1], Samson Ghilu[8], Yifei Wang[9], Steven Seaman[10], Yang Feng[10], Brad St. Croix[10], Richard Gorlick[9], Raushan Kurmasheva[8], Peter J. Houghton[8], and John M. Maris[1,2]

## ABSTRACT

**Purpose:** Patients with relapsed pediatric solid malignancies have few therapeutic options, and many of these patients die of their disease. B7-H3 is an immune checkpoint protein encoded by the *CD276* gene that is overexpressed in many pediatric cancers. Here, we investigate the activity of the B7-H3–targeting antibody–drug conjugate (ADC) m276-SL-PBD in pediatric solid malignancy patient-derived (PDX) and cell line–derived xenograft (CDX) models.

**Experimental Design:** B7-H3 expression was quantified by RNA sequencing and by IHC on pediatric PDX microarrays. We tested the safety and efficacy of m276-SL-PBD in two stages. Randomized trials of m276-SL-PBD of 0.5 mg/kg on days 1, 8, and 15 compared with vehicle were performed in PDX or CDX models of Ewing sarcoma ($N = 3$), rhabdomyosarcoma ($N = 4$), Wilms tumors ($N = 2$), osteosarcoma ($N = 5$), and neuroblastoma ($N = 12$). We then performed a single mouse trial in 47 PDX or CDX models using a single 0.5 m/kg dose of m276-SL-PBD.

**Results:** The vast majority of PDX and CDX samples studied showed intense membranous B7-H3 expression (median H-score 177, SD 52). In the randomized trials, m276-SL-PBD showed a 92.3% response rate, with 61.5% of models showing a maintained complete response (MCR). These data were confirmed in the single mouse trial with an overall response rate of 91.5% and MCR rate of 64.4%. Treatment-related mortality rate was 5.5% with late weight loss observed in a subset of models dosed once a week for 3 weeks.

**Conclusions:** m276-SL-PBD has significant antitumor activity across a broad panel of pediatric solid tumor PDX models.

## Introduction

Pediatric cancer mortality has declined by 65% since 1970 (1). A large proportion of this progress can be attributed to marked reduction in deaths from leukemia, which has been achieved through optimization of chemotherapy regimens (2). In contrast, there has been only modest improvement in survival probabilities for children, adolescents, and young adults with many high-risk solid malignancies despite dramatic intensification of cytotoxic therapy (3), such that survivors face lifelong complications due to intensive, multimodal therapy, underscoring a critical need for development of new therapies for pediatric cancer (4–6). Novel therapeutic approaches are thus required to improve outcomes for high-risk childhood solid malignancies.

While immune checkpoint inhibitors have shown remarkable efficacy in many adult solid malignancies, there has not been a significant activity signal in clinical trials for patients with pediatric solid tumors (7, 8), at least in part due to the fact that pediatric tumors generally have low mutation burdens and thus few neoantigens, and generally low expression of PD-L1 (9–11). CD19-directed chimeric antigen receptor (CAR) engineered T-cell therapy has shown remarkable efficacy in B-cell leukemias (12–14), but as yet few convincing durable responses in solid malignancies have been observed for CAR T cells targeting surface antigens relevant for pediatric solid tumors. Antibody–drug conjugates (ADC) couple the specificity of antibodies with highly potent cytotoxic agents, conferring increased potency and potential for bystander killing not seen with mAbs alone (15–18). There are currently 10 FDA-approved ADCs for a variety of human cancers, dozens in clinical development, but in children only ADCs against leukemias and lymphomas have been actively developed.

The B7-H3 protein (encoded from the *CD276* gene) is a checkpoint molecule that is highly expressed in pediatric solid tumors, with reportedly limited expression in normal tissues (19–25). Overexpression of B7-H3 is correlated with tumor progression, metastasis, and poor clinical outcome across a variety of malignancies (26, 27). mAbs

[1]Division of Oncology and Center for Childhood Cancer Research, Children's Hospital of Philadelphia, Pennsylvania. [2]Perelman School of Medicine, University of Pennsylvania, Philadelphia, Pennsylvania. [3]A.I. duPont Hospital for Children, Wilmington, Delaware. [4]NCI Cancer Therapy Evaluation Program, Bethesda, Maryland. [5]RTI International, Research Triangle Park, North Carolina. [6]Division of Anatomic Pathology, Children's Hospital of Philadelphia, Philadelphia, Pennsylvania. [7]Department of Biomedical and Health Informatics, Children's Hospital of Philadelphia, Pennsylvania. [8]Greehey Children's Cancer Research Institute, University of Texas Health Science Center at San Antonio, San Antonio, Texas. [9]Department of Pediatrics, Children's Cancer Hospital, The University of Texas MD Anderson Cancer Center, Houston, Texas. [10]Tumor Angiogenesis Unit, Mouse Cancer Genetics Program (MCGP), NCI-Frederick, Frederick, Maryland.

**Note:** Supplementary data for this article are available at Clinical Cancer Research Online (http://clincancerres.aacrjournals.org/).

N.M. Kendsersky and J. Lindsay contributed equally to this article.

**Corresponding Authors:** John M. Maris, Division of Oncology and Center for Childhood Cancer Research, Children's Hospital of Philadelphia, Philadelphia, PA 19104. Phone: 215-590-5244; E-mail: maris@chop.edu; and Peter J. Houghton, houghtonp@uthscsa.edu

Clin Cancer Res 2021;27:2938–46

**doi:** 10.1158/1078-0432.CCR-20-4221

## Translational Relevance

B7-H3 (CD276) has emerged as a promising immunotherapy target in many human malignancies. Here, we evaluated the efficacy of the B7-H3–targeted antibody–drug conjugate m276-SL-PBD in a large panel of pediatric solid tumor patient- and cell-derived xenograft models. Potent antitumor activity was observed in the majority of models studied, supporting the clinical development of m276-SL-PBD in high-risk childhood solid malignancies.

targeting B7-H3 cause limited toxicity and have demonstrated some antitumor activity in clinical trials (28, 29). Furthermore, intrathecal delivery of $^{131}$I-8H9 (omburtamab) is in late-phase clinical development for neuroblastomas with brain and/or leptomeningeal metastasis, to date showing a manageable toxicity profile with tumoricidal doses (30). Recent work has concerned development of B7-H3 CAR-T cells (23, 24), with one study demonstrating efficacy in Ewing sarcoma, osteosarcoma, and medulloblastoma xenografts (22). Finally, a pyrrolobenzodiazepine (PBD)-armed ADC against CD276 (m276-PBD, a precursor to m276-SL-PBD) showed antitumor activity in a variety of adult cancer preclinical models, including superiority over a monomethyl auristatin E (MMAE)-armed anti-CD276 ADC (31). While both PBD and MMAE are DNA-binding agents, the superiority of PBD is likely due to PBD functioning irrespective of the stage of the cell cycle, thereby eradicating both the tumor and the tumor vasculature. Together, these data suggest CD276 is a rational target for further ADC development. Here, we present results from the Pediatric Preclinical Testing Consortium (PPTC) investigation of m276-SL-PBD across a large and diverse panel of pediatric cancer patient-derived (PDX) and cell line–derived xenograft (CDX) models.

## Materials and Methods

### RNA sequencing analysis

PDX RNA sequencing (RNA-seq) data were gathered from the PPTC dataset available on cBioPortal (32). Normal tissue RNA-seq data were gathered from the Genome-Tissue Expression (GTEx) resource (https://gtexportal.org/home/). Patient tumor RNA-seq data were collected from the Treehouse Childhood Cancer Initiative (https://treehousegenomics.soe.ucsc.edu/), which included data from the Therapeutically Applicable Research to Generate Effective Treatments initiative (https://ocg.cancer.gov/programs/target). The associated data and code used to generate the figures are available in an open-access GitHub Repository at https://github.com/nathankendsersky/pptc_cd276.

### IHC

Tissue microarrays (TMA) including human normal childhood tissues, human neuroblastoma primary tumors, and PDX arrays for the histologies studied here were constructed as described previously, with normal tissues obtained from surgical or autopsy specimens at the Children's Hospital of Philadelphia (Philadelphia, PA), as described previously (33–35). Staining was performed with a polyclonal B7-H3 antibody (R&D, AF1027) at a 1:1,000 dilution. Aperio GENIE Classifier (Leica Biosystems) was used to annotate tumor regions and exclude stroma and necrosis. Tumor classification was reviewed and any discordant classifications were manually annotated by a pathologist (J. Pogoriler). For each tumor core, Aperio Membrane V9 algorithm (Leica Biosystems) was used to quantify staining intensity and percentage of tumor cells stained. H-scores were calculated by the following formula [(1 × %cells intensity = 1) + (2 × %cells intensity = 2) + (3 × %cells intensity = 3)]. Cores in which fewer than 100 cells were available for evaluation were excluded.

### ADC generation

The antibody used to create the m276-SL-PBD ADC, called m276-SL, is a modified version of the fully human m276 IgG1 antibody (31) engineered to contain four mutations (S239C, L234A/L235A/P329G) in the Fc domain (36). The S239C mutation was used for site-specific maleimide-based PBD conjugation via a dipeptide (valine-alanine) linker (36) while the LALA-PG mutations were used to prevent undesirable interactions of the ADC with Fc receptors that could potentially result in off-target killing (37). Further details about the synthesis of the modified ADC will be published separately.

### Preclinical trials

CB17SC *scid*$^{-/-}$ female (5–8 weeks) mice (Taconic Farms or ENVIGO) were used to propagate subcutaneous xenografts. All mice were maintained under barrier conditions and experiments were conducted using protocols and conditions in accordance with the Institutional Animal Care and Use Committee at The University of Texas Health San Antonio (UTHSA; San Antonio, TX), M.D. Anderson Cancer Center (Houston, TX), and the Children's Hospital of Philadelphia (Philadelphia, PA). The number of mice per group (control and treatment) was varied as indicated, with 10, 2, or 1 animal(s). For randomized controlled trials with either 10 or 2 mice per arm, 0.5 mg/kg of m276-SL-PBD or (0.5 mg/kg) of 100 μL/20 g PBS was administered intraperitoneally once a week for 3 weeks (days 1, 8, and 15). A dose of 0.5 mg/kg was chosen because it was the lowest effective dose discovered in Seaman and colleagues (31). For the single mouse trial (SMT; $N = 1$) study (38), a single dose of 0.5 mg/kg m276-SL-PBD was administered intraperitoneally. Treatment was initiated when tumor volumes reached 200 mm$^3$, and tumor volume and event-free survival (EFS) were monitored as reported previously (29).

### Statistical methods

A tumor *event* was defined as a quadrupling of tumor volume from the day of treatment initiation, where tumor volume was estimated from caliper measurements as $(4/3) \times \pi \times ((length + width)/4)^3$. The exact time to event was estimated by interpolating between the measurements directly preceding and following the event, assuming log-linear growth. Differences in EFS between experimental groups of $N > 2$ were evaluated using the Gehan–Wilcoxon test, and differences in minimum relative tumor volume (RTV; ratio of current tumor volume to volume at treatment initiation) were evaluated using the Wilcoxon rank-sum test.

Area over the curve (AOC) is the area above the RTV growth curve but below the event threshold of RTV = 4. It was calculated for each mouse using the trapezoid rule and was then divided by 4; a day of complete tumor remission, therefore, adds exactly 1 to the AOC. The AOC is correlated with time to event, but also captures the maximum extent and durability of tumor remission. It is a continuous, composite measure of tumor response over the course of the experiment and is therefore well suited for genomic analyses of association between tumor response and specific mutations.

The objective response categories are progressive disease (PD, which is subdivided among treated mice into PD without and with growth delay, PD1 and PD2, respectively), stable disease (SD), partial

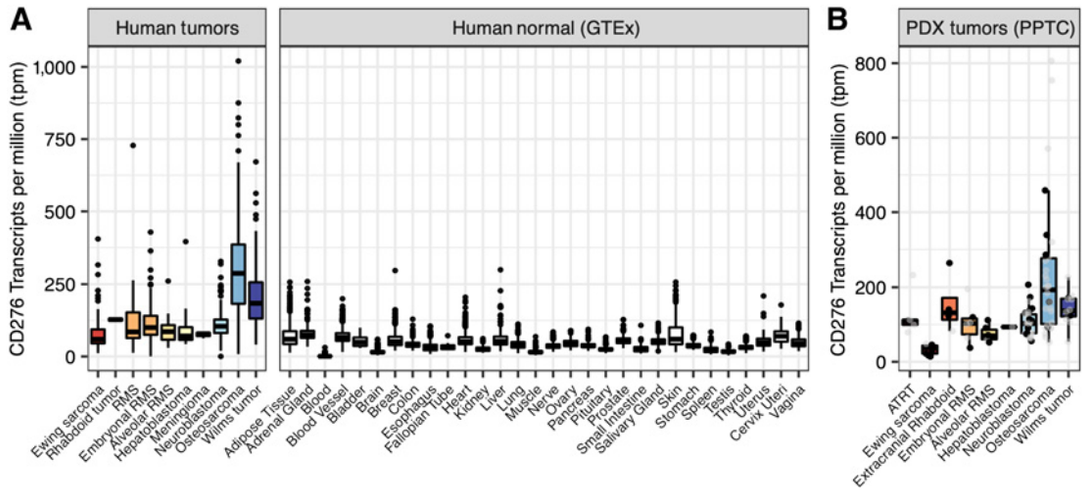


**Figure 1.**

*CD276* expression in pediatric PDX and CDX models. **A,** RNA-seq expression data for *CD276* in pediatric solid tumors (TARGET, Treehouse) and normal tissue samples (GTEx database). **B,** *CD276* mRNA expression from PPTC RNA-seq data in nine solid pediatric tumor histologies present in this study (ATRT 6; Ewing sarcoma 9; extracranial rhabdoid 4; embryonal rhabdomyosarcoma (RMS) 6; alveolar RMS 6; hepatoblastoma 1; neuroblastoma 33; osteosarcoma 30; Wilms tumor 12). Black points in **B** indicate models examined in $N > 1$ or SMT study (of 62 unique models tested, 37 had RNA-sequencing data).

response (PR), complete response (CR; no measurable tumor mass for one recording), and maintained CR (MCR; no measurable tumor mass for at least three consecutive weekly recordings) as described previously (39). Response rate is defined as the percentage of mice with PR or better. Mice experiencing a possibly treatment-related death (i.e., drug toxicity), mice with failed engraftment, and mice that unexpectedly die for reasons unrelated to treatment are excluded from statistical analyses of time to event, minimum tumor volume, and objective response.

For experiments of groups of $N = 2$ mice per group, we did not perform any statistical tests of group differences but have reported all other summary statistics. For the SMT, we report time to event, AOC, minimum RTV, and the objective response measure for each PDX or CDX model tested.

## Results

### B7-H3 is highly expressed in high-risk pediatric solid malignancies with limited normal childhood tissue expression

*CD276* mRNA was generally highly expressed in pediatric solid tumors, compared to generally low expression in a panel of 1,641 normal tissues samples from 25 organs (**Fig. 1A**). Likewise, *CD276* mRNA was highly expressed in each PDX model studied here (32). Ewing sarcoma models had the lowest median mRNA expression of *CD276* (median = 37.42 transcripts per million, TPM, normalized by trimmed mean of M-values) whereas osteosarcomas (median = 165.92 TPM) and Wilms tumors (median = 142.29 TPM) showed the highest levels of mRNA expression (**Fig. 1B**). IHC of three tumor TMAs showed strong staining across the tested PDXs (**Fig. 2A–C**). Osteosarcoma models showed the highest expression of CD276 (median H-score = 243.0). Overall, we observed a moderate correlation ($R$ = 0.527, $P$ = 7.13e-05) between mRNA (TPM) and protein expression (median H-Score; Supplementary Fig. S1). For the normal tissue array, the membrane algorithm was applied to assist in reproducible evaluation of the intensity of membranous staining, with pathologist review to determine which cell types were staining in any given tissue (Supplementary Fig. S2). Strong staining (3+) was seen in the basal layer of the epidermis of the skin. Weak (2+) staining was present in the adrenal cortex, bladder urothelium, basal layer of the esophageal epithelium, prostatic epithelium, pancreatic islet tissue, ovarian stroma, splenic stroma, and a subset of pituitary cells. Staining of the bone marrow hematopoietic cells as well as the epithelium in the ileocecum, colon, and stomach varied from negative (0) to weak (2+). Equivocal (1+) staining was present in a subset of cardiac myocytes, a subset of aortic stromal cells, a subset of gastrointestinal tract stromal cells (appendix, colon, small intestine, stomach), gallbladder epithelium, basal urothelium of the ureter, fallopian tube epithelium and subsets of cortical neurons, renal podocytes and subset of renal tubular cells, pancreatic exocrine tissue, hepatocytes, pulmonary epithelium, a subset of germinal center cells (lymph node, tonsils, spleen), salivary gland acinar cells, and a subset of developing spermatozoa. Staining was negative in other tissues including cerebellum, mature bone, skeletal muscle, and thyroid.

### m276-SL-PBD shows strong antitumor activity in pediatric PDX models

The efficacy and toxicity of m276-SL-PBD was initially evaluated in 26 pediatric PDX and CDX models in randomized controlled trial with either 10 or 2 mice per arm (**Table 1**; Supplementary Table S1). This was followed by a SMT using a single dose of m276-SL-PBD in 47 distinct models (33 PDX, 14 CDX; **Table 2**; ref. 40). m276-SL-PBD was generally well tolerated with a treatment-related mortality rate of 5.5% when administered in three weekly doses and 0% when administered as a single dose. In the randomized trials with three doses given weekly, late weight loss was observed in the Ewing sarcoma, rhabdomyosarcoma, and Wilms tumor models, but not in the osteosarcoma and neuroblastoma models (Supplementary Figs. S3–S6). No significant weight loss was observed in the SMT with a single administered dose of m276-SL-PBD (data not shown).

In the randomized trials, m276-SL-PBD induced significantly prolonged EFS in all tested mice across all models. The minimum RTV in treated mice was significantly less than the starting mean tumor

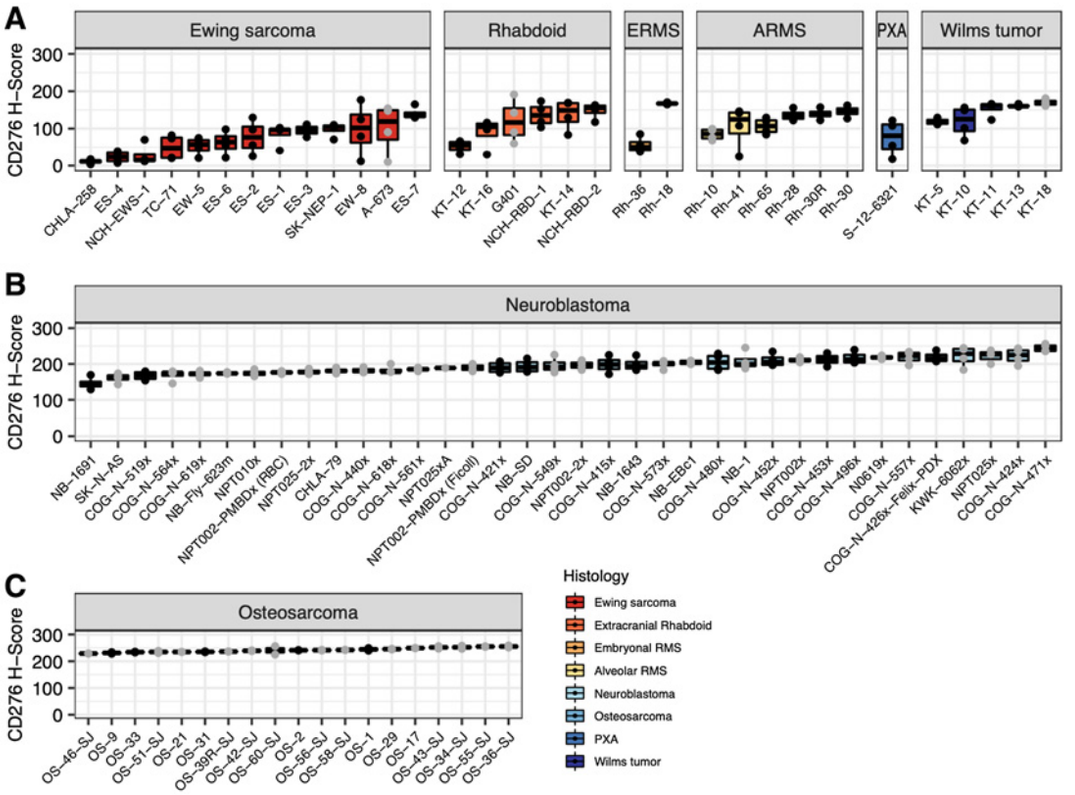


**Figure 2.**

CD276 protein expression is elevated in pediatric PDX and CDX xenografts. IHC was performed on three TMAs containing mixed PDX histologies from the SMT study (**A**), neuroblastoma models (**B**), and osteosarcoma models (**C**). Black points indicate models examined in $N > 1$ or SMT study.

volume for all models studied with the exception of one of five osteosarcoma models (OS-9) and one of 12 neuroblastoma models (NB-1691; **Fig. 3A**; Supplementary Figs. S3–S7). m276-SL-PBD showed objective responses in all models except the NB-1691 neuroblastoma model (PD1 response) and the OS-9 osteosarcoma model (SD response; **Table 1**). All Ewing, rhabdoid tumors, and Wilms models, and four of five osteosarcomas and 10 or 12 neuroblastomas showed a MCR ($N = 16$) or CR ($N = 5$). The overall response rate (PR or better) was 92.3% in the randomized trial (Supplementary Table S2). In the SMT, a single dose of m276-SL-PBD significantly prolonged EFS and decreased minimum RTV in models across all histologies tested (**Figs. 3B** and **C**; Supplementary Figs. S8 and S9). The overall response rate was 91.5% with 31 of 47 (66%) models showing a MCR (**Table 2**; Supplementary Table S2). The 10 models studied in both trial designs showed concordant responses (KT-10, KT-11, Rh-18, Rh-30, Rh-36, SK-NEP-1, ES-1, NB-1643, OS-1). Across both the randomized trial and SMT, we observed no correlation between CD276 expression (mRNA or protein) and objective response category (Supplementary Fig. S10).

## Discussion

B7-H3 is an immunomodulatory cell surface protein in the B7 superfamily, which includes other well-characterized members such as PD-L1 (41). Here we confirm and extend the previous reports of high expression on the majority of high-risk pediatric solid tumors, with significant normal childhood tissue expression by IHC limited mainly to the basal layer of skin (not previously reported), and weak expression noted in a variety of different childhood tissues (Supplementary Fig. S2; refs. 20–25). Whether or not this normal tissue expression will be a liability for an ADC that requires internalization remains unknown. In addition, B7-H3 has been shown to play a role in metastasis, and high B7-H3 expression is associated with poor outcomes across a variety of malignancies (23). However, the precise mechanisms that lead to B7-H3 overexpression and how the protein exerts its protumor function are not defined. Early studies suggested B7-H3 played a role in T-cell costimulation (42, 43). Other data point to a potential immunosuppressive, checkpoint mechanism (44, 45). Future studies are required to more precisely define the role of B7-H3 in normal human development as well as pediatric cancer tumor cell-intrinsic and extrinsic mechanisms of immune evasion.

B7-H3 has emerged as a promising immunotherapeutic target for a variety of cancers, with several immunotherapeutic platforms targeting this protein in development, including antibodies, bispecific antibodies, ADCs, and CAR T cells (22–24, 28–31). Because solid pediatric malignancies tend to have low mutational burden and immunologically cold microenvironments, which hinder adaptive immunotherapeutic approaches (9–11), ADCs may be ideal platforms for differentially expressed proteins in the plasma membrane.

We used the m276 antibody platform and covalently linked PBD with a cleavable valine-alanine linker and a drug–antibody ratio (DAR) of 2. The m276-SL-PBD ADC showed potent antitumor activity against pediatric solid xenografts at 0.5 mg/kg regardless of whether this was administered once or weekly for 3 weeks. Overall

**Table 1.** Activity of m276-SL-PBD across 26 Ewing sarcoma, rhabdomyosarcoma, osteosarcomas, and neuroblastoma models.

| Cancer type | Model | Agent | *N* | KM med (days) | EFS T - C (days) | EFS T/C | *P* value Gehan-Wilcoxon | minRTV mean ± SD | minRTV *P* value | Objective response measure |
|---|---|---|---|---|---|---|---|---|---|---|
| Ewing sarcoma | ES-1[a] | Control | 10 | 9.1 | | | | 3.450 ± 0.805 | | |
| | | mCD276-SL-PBD | 10 | >105 | >95.9 | >11.49 | $P < 0.001$ | 0.025 ± 0.070 | $P < 0.001$ | MCR |
| | ES-6[a] | Control | 10 | 15.5 | | | | 2.248 ± 0.762 | | |
| | | mCD276-SL-PBD | 10 | >41 | >25.5 | >2.64 | $P < 0.001$ | 0.000 ± 0.000 | $P < 0.001$ | CR |
| | SK-NEP-1[a] | Control | 10 | 7.6 | | | | 3.521 ± 1.254 | | |
| | | mCD276-SL-PBD | 10 | >111 | >103.4 | >14.53 | $P < 0.001$ | 0.000 ± 0.000 | $P < 0.001$ | MCR |
| Alveolar RMS (Fusion + RMS) | Rh-30 | Control | 10 | 17.2 | | | | 2.033 ± 0.558 | | |
| | | mCD276-SL-PBD | 10 | >126 | >108.8 | >7.31 | $P < 0.001$ | 0.000 ± 0.000 | $P < 0.001$ | MCR |
| | Rh-41 | Control | 10 | 12.9 | | | | 2.269 ± 0.376 | | |
| | | mCD276-SL-PBD | 10 | >105 | >92.1 | >8.15 | $P < 0.001$ | 0.000 ± 0.000 | $P < 0.001$ | MCR |
| Embryonal RMS (Fusion − RMS) | Rh-18 | Control | 10 | 15.0 | | | | 1.873 ± 0.239 | | |
| | | mCD276-SL-PBD | 10 | >119 | >104 | >7.91 | $P < 0.001$ | 0.000 ± 0.000 | $P < 0.001$ | MCR |
| | Rh-36 | Control | 10 | 4.7 | | | | 8.584 ± 2.174 | | |
| | | mCD276-SL-PBD | 10 | >105 | >100.3 | >22.14 | $P < 0.001$ | 0.000 ± 0.000 | $P < 0.001$ | MCR |
| Wilms tumor | KT-10 | Control | 10 | 13.5 | | | | 2.103 ± 0.372 | | |
| | | mCD276-SL-PBD | 10 | >98 | >84.5 | >7.26 | $P < 0.001$ | 0.000 ± 0.000 | $P < 0.001$ | MCR |
| | KT-11 | Control | 10 | 13.3 | | | | 2.123 ± 0.385 | | |
| | | mCD276-SL-PBD | 10 | >105 | >91.7 | >7.9 | $P < 0.001$ | 0.000 ± 0.000 | $P < 0.001$ | MCR |
| Osteosarcoma | OS-1 | Control | 9 | 32.3 | | | | 1.556 ± 0.244 | | |
| | | mCD276-SL-PBD | 10 | >76 | >43.7 | >2.36 | $P < 0.001$ | 0.076 ± 0.116 | $P < 0.001$ | CR |
| | OS-2 | Control | 10 | 16.3 | | | | 1.455 ± 0.186 | | |
| | | mCD276-SL-PBD | 10 | >69 | >52.7 | >4.23 | $P < 0.001$ | 0.000 ± 0.000 | $P < 0.001$ | MCR |
| | OS-9 | Control | 10 | 15.3 | | | | 2.077 ± 0.278 | | |
| | | mCD276-SL-PBD | 10 | >26 | >10.7 | >1.7 | $P < 0.001$ | 0.442 ± 0.162 | $P < 0.001$ | SD |
| | OS-31 | Control | 10 | 20.2 | | | | 1.853 ± 0.291 | | |
| | | mCD276-SL-PBD | 10 | >62 | >41.8 | >3.07 | $P < 0.001$ | 0.071 ± 0.119 | $P < 0.001$ | CR |
| | OS-33 | Control | 10 | 17.8 | | | | 1.717 ± 0.404 | | |
| | | mCD276-SL-PBD | 10 | >62 | >44.2 | >3.48 | $P < 0.001$ | 0.000 ± 0.000 | $P < 0.001$ | MCR |
| Neuroblastoma[b] | COG-N-415x | Control | 2 | 6.2 | | | | 2.052 ± 0.162 | | |
| | | mCD276-SL-PBD | 2 | 46.9 | 40.7 | 7.53 | | 0.000 ± 0.000 | | MCR |
| | COG-N-421x | Control | 2 | 21.5 | | | | 1.136 ± 0.179 | | |
| | | mCD276-SL-PBD | 2 | >101 | >79.5 | >4.69 | | 0.000 ± 0.000 | | MCR |
| | COG-N-452x | Control | 2 | 17.8 | | | | 1.069 ± 0.062 | | |
| | | mCD276-SL-PBD | 2 | >102 | >84.2 | >5.73 | | 0.000 ± 0.000 | | MCR |
| | COG-N-453x | Control | 2 | 9.8 | | | | 2.304 ± 0.323 | | |
| | | mCD276-SL-PBD | 2 | >100 | >90.2 | >10.23 | | 0.000 ± 0.000 | | MCR |
| | COG-N-480x | Control | 2 | 12.7 | | | | 1.623 ± 0.498 | | |
| | | mCD276-SL-PBD | 2 | >108 | >95.3 | >8.54 | | 0.000 ± 0.000 | | MCR |
| | COG-N-496x | Control | 2 | 9.1 | | | | 1.742 ± 0.278 | | |
| | | mCD276-SL-PBD | 2 | >43 | >33.9 | >4.75 | | 0.175 ± 0.084 | | PR |
| | COG-N-519x | Control | 2 | 12.9 | | | | 1.529 ± 0.321 | | |
| | | mCD276-SL-PBD | 2 | >101 | >88.1 | >7.82 | | 0.021 ± 0.030 | | CR |
| | COG-N-426x-Felix-PDX | Control | 2 | 11.8 | | | | 1.006 ± 0.094 | | |
| | | mCD276-SL-PBD | 2 | >26 | >14.2 | >2.2 | | 0.000 ± 0.000 | | CR |
| | NB-1643[a] | Control | 2 | 12.4 | | | | 1.016 ± 0.002 | | |
| | | mCD276-SL-PBD | 2 | >50 | >37.6 | >4.03 | | 0.122 ± 0.004 | | PR |
| | NB-1691[a] | Control | 2 | 7.3 | | | | 1.790 ± 0.119 | | |
| | | mCD276-SL-PBD | 2 | 28.8 | 21.5 | 3.95 | | 1.831 ± 0.485 | | PD1 |
| | NB-Ebc1[a] | Control | 2 | 6.8 | | | | 2.888 ± 0.698 | | |
| | | mCD276-SL-PBD | 2 | >102 | >95.2 | >15.02 | | 0.000 ± 0.000 | | MCR |
| | NB-SD[a] | Control | 2 | 19.1 | | | | 1.108 ± 0.007 | | |
| | | mCD276-SL-PBD | 2 | >64 | >44.9 | >3.36 | | 0.094 ± 0.034 | | PR |

Abbreviations: EFS T–C, difference in median time to event of treatment group compared with control; EFS T/C, ratio of median time to event of treatment group compared with control group; KM Med, Kaplan–Meier estimate of median time to event.

[a]Cell line–derived xenograft models.

[b]Neuroblastoma experiments had $N = 2$, thus *P* values are not reported.

**Table 2.** Activity of m276-SL-PBD (single administration) in a SMT.

| Cancer type | Model | Toxic death | Event | Time to event | AOC | minRTV | Objective response measure[a] |
|---|---|---|---|---|---|---|---|
| CNS ATRT | BT-29 | 0 | 0 | >112 | >84.2 | 0.000 | CR |
| | BT-35 | 0 | 1 | 65.0 | 52.8 | 0.000 | MCR |
| | BT-39 | 0 | 0 | >147 | >138.2 | 0.000 | MCR |
| | BT-40 | 0 | 0 | >107 | >104.7 | 0.000 | MCR |
| | BT-50 | 0 | 0 | >147 | >144.2 | 0.000 | MCR |
| Ewing | CHLA-258[a] | 0 | 0 | >119 | >117.2 | 0.000 | MCR |
| | ES-1[a] | 0 | 1 | 60.4 | 48.2 | 0.165 | PR |
| | ES-2[a] | 0 | 1 | 149.3 | 133.5 | 0.000 | CR |
| | ES-3[a] | 0 | 0 | >133 | >131.3 | 0.000 | MCR |
| | ES-4[a] | 0 | 0 | >147 | >146.1 | 0.000 | MCR |
| | ES-6[a] | 0 | 1 | 126.7 | 103.4 | 0.179 | PR |
| | ES-7[a] | 0 | 0 | >107 | >98.8 | 0.000 | MCR |
| | EW-5 | 0 | 1 | 18.1 | 6.2 | 2.862 | PD1 |
| | EW-8[a] | 0 | 0 | >107 | >90.0 | 0.000 | CR |
| | NCH-EWS-1 | 0 | 0 | >70 | >62.9 | 0.000 | MCR |
| | SK-NEP-1[a] | 0 | 1 | 106.2 | 81.7 | 0.000 | CR |
| | TC-71[a] | 0 | 0 | >77 | >54.5 | 0.114 | PR |
| Rhabdoid | KT-12 | 0 | 0 | >147 | >145.2 | 0.000 | MCR |
| | KT-14 | 0 | 0 | >98 | >95.7 | 0.000 | MCR |
| | KT-16 | 0 | 1 | 125.3 | 98.0 | 0.333 | PR |
| | NCH-RBD-1 | 0 | 0 | >147 | >144.9 | 0.000 | MCR |
| | NCH-RBD-2 | 0 | 0 | >70 | >69.0 | 0.000 | MCR |
| ERMS (Fusion − RMS) | IRS-56 | 0 | 0 | >119 | >116.8 | 0.000 | MCR |
| | JR-1[a] | 0 | 0 | >107 | >105.5 | 0.000 | MCR |
| | Rh-18 | 0 | 1 | 129.9 | 107.2 | 0.000 | CR |
| | Rh-36 | 0 | 0 | >147 | >145.6 | 0.000 | MCR |
| | SJR-HBO11-X | 0 | 1 | 24.7 | 13.0 | 1.299 | PD1 |
| | SJR-HBO13758-X2 | 0 | 1 | 15.8 | 6.6 | 1.942 | PD1 |
| | SMSCTR[a] | 0 | 1 | 63.2 | 45.9 | 0.177 | PR |
| ARMS (Fusion + RMS) | NCH-S13-7484 | 0 | 0 | >126 | >121.5 | 0.000 | MCR |
| | Rh-28 | 0 | 0 | >77 | >75.7 | 0.000 | MCR |
| | Rh-30 | 0 | 0 | >147 | >144.0 | 0.000 | MCR |
| | Rh-30R | 0 | 0 | >147 | >145.1 | 0.000 | MCR |
| | Rh-65 | 0 | 0 | >133 | >131.4 | 0.000 | MCR |
| | Rh-66 | 0 | 0 | >70 | >66.4 | 0.000 | MCR |
| Hepatoblastoma | CPRIT−1957 | 0 | 0 | >70 | >67.6 | 0.000 | MCR |
| Meningioma | NCH-S13-5042 | 0 | 1 | 24.5 | 12.6 | 1.272 | PD1 |
| Neuroblastoma | NB-1382[a] | 0 | 0 | >107 | >93.3 | 0.000 | MCR |
| | NB-1643[a] | 0 | 0 | >107 | >104.0 | 0.000 | MCR |
| Osteosarcoma | CPRIT−0522 − 000 | 0 | 0 | >133 | >122.7 | 0.000 | CR |
| | OS-1 | 0 | 0 | >107 | >102.2 | 0.000 | MCR |
| PXA | S-12-6321 | 0 | 0 | >147 | >145.0 | 0.000 | MCR |
| Wilms | CPRIT−1960 | 0 | 0 | >70 | >66.7 | 0.000 | CR |
| | KT-10 | 0 | 0 | >147 | >146.1 | 0.000 | MCR |
| | KT-11 | 0 | 0 | >133 | >132.1 | 0.000 | MCR |
| | KT-13 | 0 | 0 | >147 | >144.3 | 0.000 | MCR |
| | KT-5 | 0 | 0 | >70 | >68.0 | 0.000 | MCR |

Note: SMT experiments had $N = 1$, thus $P$ values are not reported. m276-SL-PBD was given as a single administration at 0.5 mg/kg i.p.
Abbreviation: PXA, pleiomorphic xanthoastrocytoma.
[a]Cell line–derived xenograft models.

response rates above 90% in both the randomized and SMTs, with limited observed toxicity, is an encouraging signal for clinical development. Importantly, m276 binds human and mouse B7-H3 with equal affinity (31), which further supports a potential therapeutic index in pediatric patients. The weight loss in the multidose experiments in some of the sarcoma and Wilms models may be due to a cumulative effect of PBD, as has been previously observed in clinical trials of PBD-family agents (46), as well as the sensitivity of CB17SC *scid*$^{-/-/-}$animals to DNA-damaging agents. No skin toxicity was observed in the mice treated in this study.

Our results with m276-SL-PBD confirm the utility of the SMT design as an efficient and accurate design for screening large panels of xenograft models. A retrospective analysis of 67 agents tested by the Pediatric Preclinical Testing Program using $N = 8$ or 10 mice per group

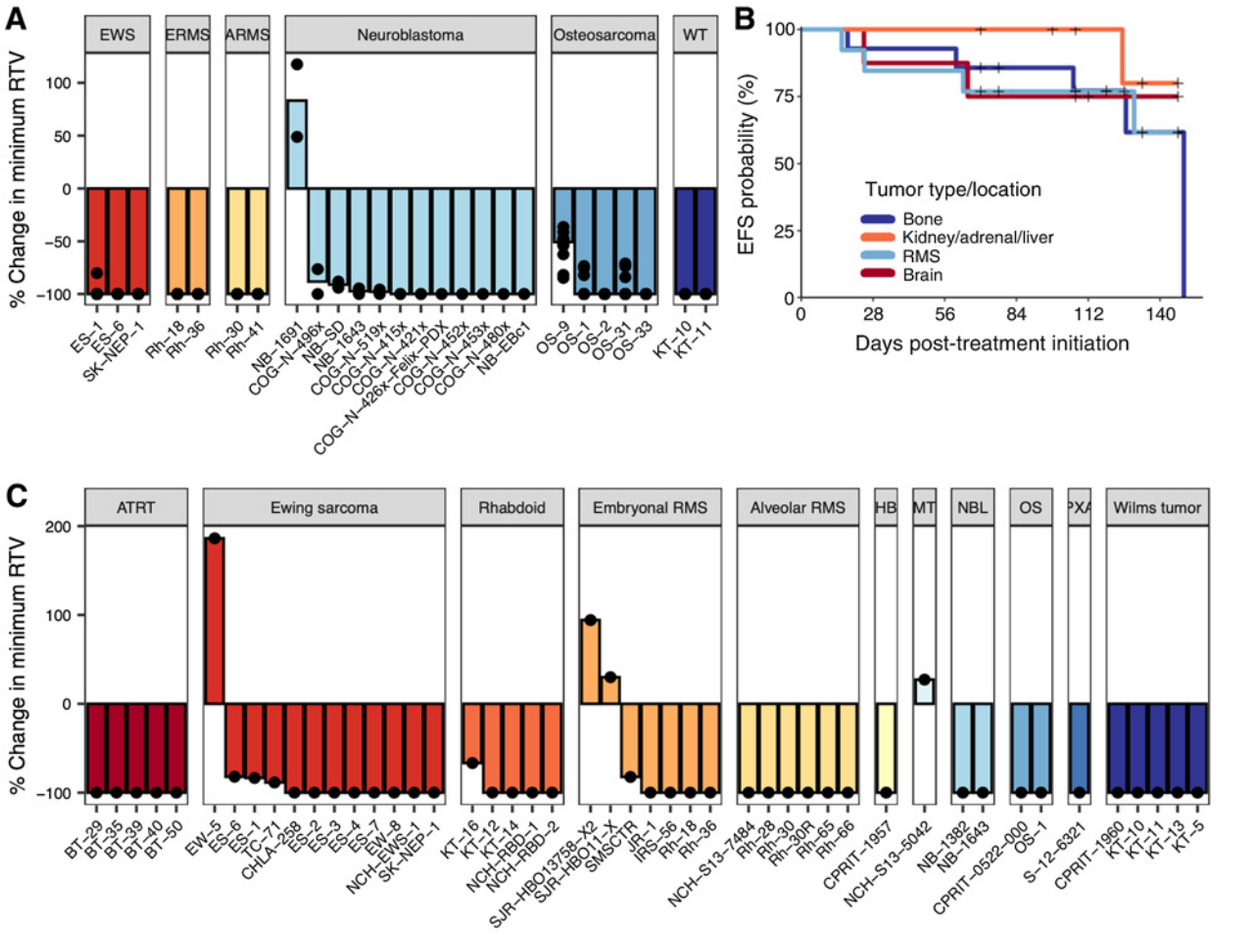


**Figure 3.**

Tumor volume and EFS with m276-SL-PBD administration. **A,** Waterfall plots for Ewing sarcoma (10 mice per model), rhabdomyosarcoma (10 mice per model), osteosarcoma (10 mice per model), and neuroblastoma (2 mice per model) PDX/CDXs. Bars represent median percent change in minimum relative tumor volume in treated mice. **B,** Kaplan–Meier plot of all 47 single mouse experiments ($N = 1$) with "+" representing right-censored data. Colors represent the location of tumor origin [bone includes osteosarcoma (2 models) and Ewing sarcoma (12 models); kidney/adrenal/liver includes neuroblastoma (2 models), extracranial rhabdoid (5 models), hepatoblastoma (1 model), and Wilms tumor (5 models); RMS includes alveolar (6 models) and embryonal RMS (7 models); brain includes ATRT (5 models), PXA (1 model), and meningioma (1 model)]. **C,** Waterfall plots for models in SMT. Bars represent median percent change in minimum relative tumor volume in treated mice.

evaluated whether a single mouse chosen at random predicted the group median objective response. Out of 2,134 total comparisons, the single mouse matched the group median response 78% of the time and fell within one response category away 95% of the time (40). More recent work analyzed 30 agents tested by the PPTC from 2015 to 2018 and observed exact and near match rates of 82% and 94%, respectively (47).

It is very likely that ADC payloads may need to be tailored to potentially unique cytotoxic vulnerabilities and mechanisms or drug resistance in childhood cancer. Especially in the relapse setting after dose intensive chemotherapy, many of the favored payloads in licensed ADCs like DM1 may not be ideal as they are substrates for P-glycoprotein and other drug efflux pumps. In addition, it was recently demonstrated that m276-SL-PBD confers advantages over m276-MMAE due to PBD-mediated eradication of tumor-associated vasculature in adult tumor xenograft models (31). However, ADCs with PBD-family cytotoxic agents have shown toxicity in the clinic (48), and the antitumor activity seen at 0.5 mg/kg must be viewed in the context of a dose and schedule that can be achieved in the clinic. It is reassuring in our study that deescalation from 0.5 mg/kg once a week for 3 weeks to a single 0.5 mg/kg dose had no impact on antitumor activity, suggesting that with an ideal target, stable linker, and brisk internalization kinetics, PBD containing ADCs directed at B7-H3 can be developed clinically. Our data support further development of B7-H3 ADCs for childhood cancers.

## Authors' Disclosures

S. Seaman reports a patent for 62/947.135 pending and a patent 10604582 issued. Y. Feng reports a patent for 62/947135 pending. B. St. Croix reports a patent for 62/947,135 pending and a patent 10604582 issued. No disclosures were reported by the other authors.

## Authors' Contributions

**N.M. Kendsersky:** Data curation, visualization, writing–original draft, writing–review and editing. **J.Lindsay:** Data curation, visualization, writing–original draft, writing–review and editing. **E.A. Kolb:** Conceptualization, funding acquisition,

writing–review and editing. **M.A. Smith:** Conceptualization, resources, formal analysis, supervision, writing–original draft, project administration, writing–review and editing. **B.A. Teicher:** Conceptualization, writing–review and editing. **S.W. Erickson:** Data curation, formal analysis, visualization. **E.J. Earley:** Data curation, formal analysis, visualization. **Y.P. Mosse:** Conceptualization, supervision, investigation, writing–review and editing. **D. Martinez:** Data curation, formal analysis, investigation, visualization. **J. Pogoriler:** Data curation, formal analysis, investigation, visualization. **K. Krytska:** Data curation, formal analysis, investigation. **K. Patel:** Data curation, formal analysis, visualization, methodology. **D. Groff:** Data curation, investigation. **M. Tsang:** Data curation, investigation. **S. Ghilu:** Data curation, investigation. **Y. Wang:** Data curation, investigation, methodology. **S. Seaman:** Conceptualization, resources. **Y. Feng:** Resources. **B. St. Croix:** Conceptualization, resources, writing–original draft, writing–review and editing. **R. Gorlick:** Conceptualization, resources, data curation, formal analysis, supervision, funding acquisition, writing–review and editing. **R. Kurmasheva:** Conceptualization, supervision, writing–original draft, writing–review and editing. **P.J. Houghton:** Conceptualization, resources, supervision, funding acquisition, investigation, writing–original draft, project administration, writing–review and editing. **J.M. Maris:** Conceptualization, resources, supervision, funding acquisition, investigation, writing–original draft, project administration, writing–review and editing.

## Acknowledgments

This work was supported by NCI U01 CA199287 (to J.M. Maris), NCI R35 CA220500 (to J.M. Maris), NCI U01 CA199221 (to Richard G. Gorlick), NCI U01 CA199297 (to P.J. Houghton), CPRIT RP160716 (to P.J. Houghton), NCI F31 CA239424 (to N.M. Kendsersky), NCI F31 CA254244 (to J. Lindsay), NCI U01 CA199222 (to Gregory J. Gatto), and the Giulio D'Angio Endowed Chair (to J.M. Maris).

The costs of publication of this article were defrayed in part by the payment of page charges. This article must therefore be hereby marked *advertisement* in accordance with 18 U.S.C. Section 1734 solely to indicate this fact.

Received November 3, 2020; revised January 7, 2021; accepted February 15, 2021; published first February 22, 2021.

## References

1. Siegel RL, Miller KD, Jemal A. Cancer statistics, 2019. CA Cancer J Clin 2019;69:7–34.
2. Hunger SP, Mullighan CG. Acute lymphoblastic leukemia in children. N Engl J Med 2015;373:1541–52.
3. Perkins SM, Shinohara ET, DeWees T, Frangoul H. Outcome for children with metastatic solid tumors over the last four decades. PLoS One 2014;9:e100396.
4. Diller L, Chow EJ, Gurney JG, Hudson MM, Kadin-Lottick NS, Kawashima TI, et al. Chronic disease in the childhood cancer survivor study cohort: a review of published findings. J Clin Oncol 2009;27:2339–55.
5. Oeffinger KC, Hudson MM. Long-term complications following childhood and adolescent cancer: foundations for providing risk-based health care for survivors. CA Cancer J Clin 2004;54:208–36.
6. Hudson MM. Survivors of childhood cancer: coming of age. Hematol Oncol Clin North Am 2008;22:211–31.
7. Geoerger B, Zwaan CM, Marshall LV, Michon J, Bourdeaut F, Casanova M, et al. Atezolizumab for children and young adults with previously treated solid tumours, non-Hodgkin lymphoma, and Hodgkin lymphoma (iMATRIX): a multicentre phase 1–2 study. Lancet Oncol 2020;21:134–44.
8. Davis KL, Fox E, Merchant MS, Reid JM, Kudgus RA, Liu X, et al. Nivolumab in children and young adults with relapsed or refractory solid tumours or lymphoma (ADVL1412): a multicentre, open-label, single-arm, phase 1–2 trial. Lancet Oncol 2020;21:541–50.
9. Majzner RG, Heitzeneder S, Mackall CL. Harnessing the immunotherapy revolution for the treatment of childhood cancers. Cancer Cell 2017;31:476–85.
10. Majzner RG, Simon JS, Grosso JF, Martinez D, Pawel BR, Santi M, et al. Assessment of programmed death-ligand 1 expression and tumor-associated immune cells in pediatric cancer tissues. Cancer 2017;123:3807–15.
11. Davis KL, Fox E, Reid JM, Liu X, Minard CG, Weigel B, et al. ADVL1412: Initial results of a phase I/II study of nivolumab and ipilimumab in pediatric patients with relapsed/refractory solid tumors—A COG study. J Clin Oncol 35: 15s, 2017 (suppl; abstr 10526).
12. Lee DW, Kochenderfer JN, Stetler-Stevenson M, Cui YK, Delbrook C, Feldman SA, et al. T cells expressing CD19 chimeric antigen receptors for acute lymphoblastic leukaemia in children and young adults: a phase 1 dose-escalation trial. Lancet 2015;385:517–28.
13. Maude SL, Frey N, Shaw PA, Aplenc R, Barrett DM, Bunin NJ, et al. Chimeric antigen receptor T cells for sustained remissions in leukemia. N Engl J Med 2014;371:1507–17.
14. Gardner R, Wu D, Cherian S, Fang M, Hanafi LA, Finney O, et al. Acquisition of a CD19-negative myeloid phenotype allows immune escape of MLL-rearranged B-ALL from CD19 CAR-T-cell therapy. Blood 2016;127:2406–10.
15. de Goeij BECG, Lambert JM. New developments for antibody-drug conjugate-based therapeutic approaches. Curr Opin Immunol 2016;40:14–23.
16. Diamantis N, Banerji U. Antibody-drug conjugates–an emerging class of cancer treatment. Br J Cancer. 2016;114:362–7.
17. Beck A, Goetsch L, Dumontet C, Corvaïa N. Strategies and challenges for the next generation of antibody-drug conjugates. Nat Rev Drug Discov 2017;16:315–37.
18. Kovtun YV, Goldmacher VS. Cell killing by antibody-drug conjugates. Cancer Lett 2007;255:232–40.
19. Lee YH, Martin-Orozco N, Zheng P, Li J, Zhang P, Tan H, et al. Inhibition of the B7-H3 immune checkpoint limits tumor growth by enhancing cytotoxic lymphocyte function. Cell Res 2017;27:1034–45.
20. Wang L, Zhang Q, Chen W, Shan B, Ding Y, Zhang G, et al. B7-H3 is overexpressed in patients suffering osteosarcoma and associated with tumor aggressiveness and metastasis. PLoS One 2013;8:e70689.
21. Zhou Z, Luther N, Ibrahim GM, Hawkins C, Vibhakar R, Handler MH, et al. B7-H3, a potential therapeutic target, is expressed in diffuse intrinsic pontine glioma. J Neurooncol 2013;111:257–64.
22. Majzner RG, Theruvath JL, Nellan A, Heitzeneder S, Cui Y, Mount CW, et al. CAR T cells targeting B7-H3, a pan-cancer antigen, demonstrate potent preclinical activity against pediatric solid tumors and brain tumors. Clin Cancer Res 2019;25:2560–74.
23. Du H, Hirabayashi K, Ahn S, Kren NP, Montgomery SA, Wang X, et al. Antitumor responses in the absence of toxicity in solid tumors by targeting B7-H3 via chimeric antigen receptor T cells. Cancer Cell 2019;35:221–37.
24. Nguyen P, Okeke E, Clay M, Haydar D, Justice J, O'Reilly C, et al. Route of 41BB/41BBL costimulation determines effector function of B7-H3-CAR.CD28ζ T cells. Mol Ther Oncolytics 2020;18:202–14.
25. Modak S, Kramer K, Gultekin SH, Guo HF, Cheung NKV. Monoclonal antibody 8H9 targets a novel cell surface antigen expressed by a wide spectrum of human solid tumors. Cancer Res 2001;61:4048–54.
26. Tekle C, Nygren MK, Chen YW, Dybsjord I, Nesland JM, Mælandsmo GM, et al. B7-H3 contributes to the metastatic capacity of melanoma cells by modulation of known metastasis-associated genes. Int J Cancer 2012;130:2282–90.
27. Ye Z, Zheng Z, Li X, Zhu Y, Zhong Z, Peng L, et al. B7-H3 overexpression predicts poor survival of cancer patients: a meta-analysis. Cell Physiol Biochem 2016;39:1568–80.
28. Loo D, Alderson RF, Chen FZ, Huang L, Zhang W, Gorlatov S, et al. Development of an Fc-enhanced anti-B7-H3 monoclonal antibody with potent antitumor activity. Clin Cancer Res 2012;18:3834–45.
29. Powderly J, Cote G, Flaherty K, Szmulewitz RZ, Ribas A, Weber J, et al. Interim results of an ongoing phase I, dose escalation study of MGA271 (Fc-optimized humanized anti-B7-H3 monoclonal antibody) in patients with refractory B7-H3-expressing neoplasms or neoplasms whose vasculature expresses B7-H3. J Immunother Cancer 2015;3:O8.
30. Kramer K, Kushner BH, Modak S, Pandit-Taskar N, Smith-Jones P, Zanzonico P, et al. Compartmental intrathecal radioimmunotherapy: results for treatment for metastatic CNS neuroblastoma. J Neurooncol 2010;97:409–18.
31. Seaman S, Zhu Z, Saha S, Zhang XM, Yang MY, Hilton MB, et al. Eradication of tumors through simultaneous ablation of CD276/B7-H3-positive tumor cells and tumor vasculature. Cancer Cell 2017;31:501–15.
32. Rokita JL, Rathi KS, Cardenas MF, Upton KA, Jayaseelan J, Cross KL, et al. Genomic profiling of childhood tumor patient-derived xenograft models to enable rational clinical trial design. Cell Rep 2019;29:1675–89.
33. Kononen J, Bubendorf L, Kallioniemi A, Bärlund M, Schraml P, Leighton S, et al. Tissue microarrays for high-throughput molecular profiling of tumor specimens. Nat Med 1998;4:844–7.

34. Pilla D, Bosisio FM, Marotta R, Faggi S, Forlani P, Falavigna M, et al. Tissue microarray design and construction for scientific, industrial and diagnostic use. J Pathol Inform 2012;3:42.
35. Bosse KR, Raman P, Zhu Z, Lane M, Martinez D, Heitzeneder S, et al. Identification of GPC2 as an oncoprotein and candidate immunotherapeutic target in high-risk neuroblastoma. Cancer Cell 2017;32:295–309.
36. Jeffrey SC, Burke PJ, Lyon RP, Meyer DW, Sussman D, Anderson M, et al. A potent anti-CD70 antibody-drug conjugate combining a dimeric pyrrolobenzodiazepine drug with site-specific conjugation technology. Bioconjug Chem 2013;24:1256–63.
37. Lo M, Kim HS, Tong RK, Bainbridge TW, Vernes JM, Zhang Y, et al. Effector-attenuating substitutions that maintain antibody stability and reduce toxicity in mice. J Biol Chem 2017;292:3900–8.
38. Ghilu S, Li Q, Fontaine SD, Santi D V., Kurmasheva RT, Zheng S, et al. Prospective use of the single-mouse experimental design for the evaluation of PLX038A. Cancer Chemother Pharmacol 2020;85:251–63.
39. Robles AJ, Kurmasheva RT, Bandyopadhyay A, Phelps DA, Erickson SW, Lai Z, et al. Evaluation of eribulin combined with irinotecan for treatment of pediatric cancer xenografts. Clin Cancer Res 2020;26:3012–23.
40. Murphy B, Yin H, Maris JM, Kolb EA, Gorlick R, Reynolds CP, et al. Evaluation of alternative *in vivo* drug screening methodology: a single mouse analysis. Cancer Res 2016;76:5798–809.
41. Collins M, Ling V, Carreno BM. The B7 family of immune-regulatory ligands. Genome Biol 2005;6:223.
42. Chapoval AI, Ni J, Lau JS, Wilcox RA, Flies DB, Liu D, et al. B7-H3: a costimulatory molecule for T cell activation and IFN-γ production. Nat Immunol 2001;2:269–74.
43. Luo L, Chapoval AI, Flies DB, Zhu G, Hirano F, Wang S, et al. B7-H3 enhances tumor immunity *in vivo* by costimulating rapid clonal expansion of antigen-specific CD8 + cytolytic T cells. J Immunol 2004;173:5445–50.
44. Veenstra RG, Flynn R, Kreymborg K, McDonald-Hyman C, Saha A, Taylor PA, et al. B7-H3 expression in donor T cells and host cells negatively regulates acute graft-versus-host disease lethality. Blood 2015;125:3335–46.
45. Steinberger P, Majdic O, Derdak SV, Pfistershammer K, Kirchberger S, Klauser C, et al. Molecular characterization of human 4Ig-B7-H3, a member of the B7 family with four Ig-like domains. J Immunol 2004;172:2352–9.
46. Hartley JA. The development of pyrrolobenzodiazepines as antitumour agents. Expert Opin Investig Drugs 2011;20:733–44.
47. Earley E, Gorlick R, Houghton PJ, Maris JM, Li X-N, Lock RB, et al. Re-evaluating sample sizes in preclinical testing of patient-derived xenografts [abstract]. In: Proceedings of the American Association for Cancer Research Annual Meeting 2019; 2019 Mar 29–Apr 3; Atlanta, GA. Philadelphia (PA): AACR; Cancer Res 2019;79(13 Suppl):Abstract nr LB-321.
48. Saber H, Simpson N, Ricks TK, Leighton JK. An FDA oncology analysis of toxicities associated with PBD-containing antibody-drug conjugates. Regul Toxicol Pharmacol 2019;107:104429.